



CHORUS

This is the accepted manuscript made available via CHORUS. The article has been published as:

Low-symmetry monoclinic ferroelectric phase stabilized by
oxygen octahedra rotations in strained
 $\text{Eu}_x\text{Sr}_{1-x}\text{TiO}_3$ thin films

Anna N. Morozovska, Yijia Gu, Victoria V. Khist, Maya D. Glinchuk, Long-Qing Chen,
Venkatraman Gopalan, and Eugene A. Eliseev

Phys. Rev. B **87**, 134102 — Published 10 April 2013

DOI: [10.1103/PhysRevB.87.134102](https://doi.org/10.1103/PhysRevB.87.134102)

Low-symmetry monoclinic ferroelectric phase stabilized by oxygen octahedra rotation in strained $\text{Eu}_x\text{Sr}_{1-x}\text{TiO}_3$ thin films

Anna N. Morozovska^{1,2}, Yijia Gu³, Victoria V. Khist², Maya D. Glinchuk², Long-Qing Chen^{3*}, Venkatraman Gopalan^{3†}, and Eugene A. Eliseev^{2‡}

¹ Institute of Physics, NAS of Ukraine, 46, pr. Nauki, 03028 Kiev, Ukraine

²Institute for Problems of Materials Science, NAS of Ukraine, Krjijanovskogo 3, 03142 Kiev, Ukraine

³Department of Materials Science and Engineering, Pennsylvania State University, University Park, Pennsylvania 16802, USA

Using Landau-Ginzburg-Devonshire theory and phase-field modeling, we explore the complex interplay between a structural order parameter (oxygen octahedron rotation) and polarization in $\text{Eu}_x\text{Sr}_{1-x}\text{TiO}_3$ thin films. Under a biaxially tensile strain, a low symmetry monoclinic phase with in-plane ferroelectric polarization is found to be stabilized by antiferrodistortive oxygen octahedra tilts. The monoclinic phase is stable over a wide temperature range. It is characterized by a large number of energetically equivalent polar and structural twin domains. This work demonstrates the development of a spontaneous polarization, and piezo- and pyro-electricity in a ferroelastic twin boundary arising from flexoelectric coupling and rotostriction.

*qc3@ems.psu.edu

†vxg8@psu.edu

‡eugene.a.eliseev@gmail.com

I. INTRODUCTION

Epitaxial strains imposed on commensurate complex oxide thin films by substrates can lead to the emergence of a broad range of new properties [1] such as ferroelectricity [2, 3], magnetism [4], octahedral tilts [5], and multiferroicity [6] as well as of new phases with strong polar or magnetic long-range order which are absent in the corresponding bulk ferroelastics and quantum paraelectrics [1-5, 7].

As a classical example, SrTiO₃ has been extensively studied during the last a few decades. Bulk SrTiO₃ is a nonmagnetic quantum paraelectric [8] with antiferrodistortive (AFD) structural order below 105 K [9, 10, 11]. However, strained SrTiO₃ films have been shown to possess a wide range of intriguing properties, including octahedral tilts and ferroelectricity at high temperature [7, 12, 13], superconductivity [14], and surprisingly, magnetism [15], whose origin remains uncertain [16]. Another similar material that is relatively new and actively studied is EuTiO₃. The bulk quantum paraelectric EuTiO₃ is a low temperature antiferromagnet [17, 18]. It exhibits an antiferrodistortion transition at 281 K [19, 20, 21, 22, 23] and is paraelectric at high temperatures. The strained EuTiO₃ films, surprisingly, become strong ferroelectric ferromagnets under epitaxial strains exceeding 1% [24, 25, 26].

The main focus of this work is on much less studied strained films of quantum paraelectric Eu_xSr_{1-x}TiO₃. Since Eu_xSr_{1-x}TiO₃ films are solid solutions of EuTiO₃ and SrTiO₃, they may exhibit not only all the interesting structural and polar mode interactions of individual EuTiO₃ and SrTiO₃ films but also new phenomena and properties. There has been one experimental study on the structural AFD and other physical properties of bulk solid solution Eu_xSr_{1-x}TiO₃[27]. Theoretically, possible multiferroic properties of Eu_xSr_{1-x}TiO₃ nanotubes and nanowires [28] have been predicted using Landau-Ginzburg-Devonshire (LGD) theory. However, in [28], the structural AFD order parameter was considered as a scalar while the true AFD order parameter is an axial vector describing the oxygen octahedral tilt [29]. The vector nature of the AFD order parameter can strongly influence the phase stability, polar and pyroelectric properties of quantum paraelectrics [11, 30] at interfaces [31] or in thin film bulk [7, 13, 32].

Phase diagrams of strained films are usually complicated by new phases, which are absent in their bulk counterparts. Among these emergent new phases, low symmetry monoclinic phases are of particular interest due to the relative large number of possible ferroelectric and ferroelastic twin variants and wall orientations compared to higher symmetry phases, which give rise to possible dramatic enhancements in piezoelectric coefficients. Monoclinic phases with in-plane and out-of-plane polarization components of different amplitudes have been predicted theoretically in epitaxial BaTiO₃ films [33, 34, 35]. In the strained incipient ferroelectric SrTiO₃ films only tetragonal and orthorhombic phases were shown to be stable [7, 13]. However, the addition of Eu

to SrTiO₃ thin films may result in the stabilization of monoclinic phases. On the other hand, flexoelectric coupling with rotostriction effect may further enrich the behaviour in the Eu_xSr_{1-x}TiO₃ solid solution systems. It was theoretically shown that flexoelectric coupling combined with a rotostriction effect can lead to a spontaneous polarization within ferroelastic twin walls [30] and the wall – surface junctions [36]. The predicted interfacial ferroelectric phase was recently validated by experimental measurements [37] of domain wall damping and elastic softening of twin walls in SrTiO₃.

Here we study the long-range structural and polar ordering as well as the phase diagrams of Eu_xSr_{1-x}TiO₃ thin strained films using LGD theory and phase-field modeling. We focus on the origin of a low symmetry ferroelectric monoclinic phase, the stability of which is found to be related to the Eu content and the flexo-roto coupling that appears at the twin walls. This paper is organized as follows. The LGD potential for Eu_xSr_{1-x}TiO₃ is presented in Section II. Phase diagrams, structural and polar properties of Eu_xSr_{1-x}TiO₃ thin films are analyzed in Section III. Flexo-roto effects at elastic twin walls are studied in Section IV. Results are summarized in Section V. Material parameters of Eu_xSr_{1-x}TiO₃ and calculation details are given in the Supplementary Materials.

II. LANDAU-GINZBURG-DEVONSHIRE POTENTIAL FOR Eu_xSr_{1-x}TiO₃

Let us consider a short-circuited Eu_xSr_{1-x}TiO₃ film of thickness h that is clamped on to a rigid substrate (**Fig.1**). The lattice mismatch between the film and substrate leads to an in-plane strains u_m at the interface. Following Pertsev et al [33] the misfit strain can be calculated as $u_m = (b - a_0)/b$, where b is the substrate lattice parameter and a_0 is the cell constant of the free standing film extrapolated to a cubic phase.

AFD structural order is characterized by the spontaneous displacement of oxygen atoms, that can also be viewed as oxygen octahedron rotation (measured as displacement of oxygen ion or “tilts”), described by an axial vector Φ_i ($i=1, 2, 3$) [29]. Polarization is described by vector P_i . In this article, we only focus on the polar structural subsystem at temperatures higher than 50 K. Magnetic properties of EuTiO₃ at lower temperatures have been discussed elsewhere [24-26, 38].

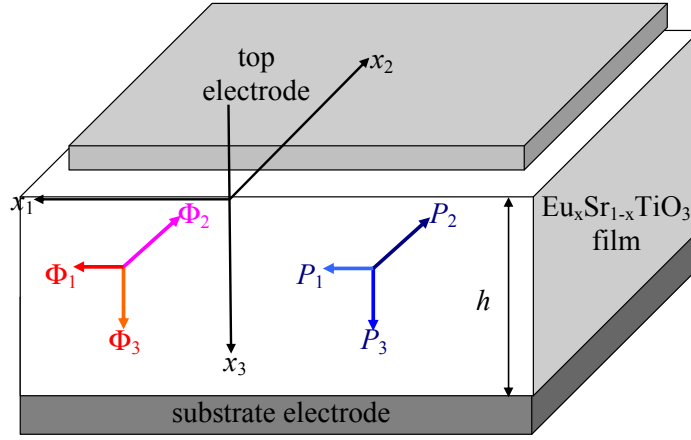


Figure 1. Schematics of a short-circuited $\text{Eu}_x\text{Sr}_{1-x}\text{TiO}_3$ film clamped on a rigid substrate.

Gibbs potential density of $\text{Eu}_x\text{Sr}_{1-x}\text{TiO}_3$ solid solution as a function of polarization and oxygen octahedra tilt vectors is written as [28]:

$$G = G_S + \int_0^h (G_{grad} + G_{flexo} + G_{elastic} + G_{P\Phi}) dx_3 \quad (1)$$

where $G_S = a_i^S (P_i^2(0) + P_i^2(h)) + b_i^S (\Phi_i^2(0) + \Phi_i^2(h))$ is the surface contribution;

$G_{grad} = \frac{g_{ijkl}}{2} \left(\frac{\partial P_i}{\partial x_j} \frac{\partial P_k}{\partial x_l} \right) + \frac{v_{ijkl}}{2} \left(\frac{\partial \Phi_i}{\partial x_j} \frac{\partial \Phi_k}{\partial x_l} \right)$ is the gradient term, and

$G_{flexo} = \frac{F_{ijkl}}{2} \left(\sigma_{ij} \frac{\partial P_k}{\partial x_l} - P_k \frac{\partial \sigma_{ij}}{\partial x_l} \right)$ is the flexoelectric term. F_{ijkl} is the forth-rank tensor of

flexoelectric coupling that was determined experimentally for SrTiO_3 in a wide temperature range by Zubko et al [39]. $G_{elastic}$ is elastic contribution, and $G_{P\Phi}$ is polarization-and-tilt-dependent

term. The form of $G_{grad} + G_S$ is the same as listed in Ref.[38]. The elastic contribution is

$G_{elastic} = -s_{ijkl} \sigma_{ij} \sigma_{kl} / 2$, where $s_{ijkl}(x) = x s_{ijkl}^{\text{EuTiO}_3} + (1-x) s_{ijkl}^{\text{SrTiO}_3}$ are elastic compliances; σ_{ij} is the

elastic stress tensor. The polarization and structural parts of the 2-4-power Landau-potential density for cubic m3m parent phase is [28]:

$$G_{P\Phi} = \left(\begin{aligned} &\alpha_p P_i^2 + \beta_{Pij} P_i^2 P_j^2 - Q_{ijkl} \sigma_{ij} P_k P_l + \alpha_\Phi \Phi_i^2 \\ &+ \beta_{\Phi ij} \Phi_i^2 \Phi_j^2 - R_{ijkl} \sigma_{ij} \Phi_k \Phi_l + \frac{\xi_{ik}}{2} \Phi_i^2 P_k^2 \end{aligned} \right) \quad (2)$$

The biquadratic coupling between the structural order parameter Φ_i and polarization components

P_i is regarded as Houchmandazeh-Laizerowicz-Salje ξ coupling which is defined by the tensor ξ_{ik}

[11, 40, [41]. And this coupling was considered as the reason for the appearance of magnetization

inside a ferromagnetic domain wall in a non-ferromagnetic media [42]. Both biquadratic coupling tensor and higher order expansion coefficients are regarded composition dependent,

$$\text{i.e. } \beta_{p,\Phi}(x) = x\beta_{p,\Phi}^{\text{EuTiO}_3} + (1-x)\beta_{p,\Phi}^{\text{SrTiO}_3} \quad \text{and} \quad \xi_{ij}(x) = x\xi_{ij}^{\text{EuTiO}_3} + (1-x)\xi_{ij}^{\text{SrTiO}_3} .$$

$Q_{ijkl}(x) = xQ_{ijkl}^{\text{EuTiO}_3} + (1-x)Q_{ijkl}^{\text{SrTiO}_3}$ and $R_{ijkl}(x) = xR_{ijkl}^{\text{EuTiO}_3} + (1-x)R_{ijkl}^{\text{SrTiO}_3}$ are the electrostriction and rotostriction tensors components respectively, which are also assumed to depend linearly on the composition x . Coefficient $\alpha_p(T, x)$ depends on the temperature T in accordance with Barrett law [43] and composition x of $\text{Eu}_x\text{Sr}_{1-x}\text{TiO}_3$ solid solution as

$$\alpha_p(T, x) = x\alpha_p^{\text{EuTiO}_3}(T) + (1-x)\alpha_p^{\text{SrTiO}_3}(T) \quad (3a)$$

$$\alpha_p(T) = \alpha_T^{(P)}(T_q^{(P)}/2) \left(\coth(T_q^{(P)}/2T) - \coth(T_q^{(P)}/2T_c^{(P)}) \right). \quad (3b)$$

Temperature $T_q^{(P)}$'s are so-called quantum vibration temperatures for SrTiO_3 and EuTiO_3 respectively, which are related to polar modes. Temperature $T_c^{(P)}$'s are the ‘‘effective’’ Curie temperatures corresponding to polar soft modes in bulk EuTiO_3 and SrTiO_3 .

The nonlinear composition dependence of the transition temperature between cubic non-AFD and tetragonal AFD phases, which was experimentally measured by Zurab Guguchia et al [27], is included in Eq.(3b) as $T_S(x) \approx 113.33 + 390.84x - 621.21x^2 + 398.87x^3$ [44]. To account for the experiment and Barrett law, the dependence of coefficient $\alpha_\Phi(T, x)$ on temperature and composition x of $\text{Eu}_x\text{Sr}_{1-x}\text{TiO}_3$ solid solution is written as

$$\alpha_\Phi(T, x) = \alpha_T^{(\Phi)}(x) \left(T_q^{(\Phi)}(x)/2 \right) \left(\coth(T_q^{(\Phi)}(x)/2T) - \coth(T_q^{(\Phi)}(x)/2T_S(x)) \right) \quad (4)$$

To determine other parameters in Eq.(4) we used linear extrapolations, e.g., $\alpha_T^{(\Phi)}(x) = x \cdot \alpha_{T\Phi}^{\text{EuTiO}_3} + (1-x)\alpha_{T\Phi}^{\text{SrTiO}_3}$ and $T_q^{(\Phi)}(x) = x \cdot T_{q\Phi}^{\text{EuTiO}_3} + (1-x)T_{q\Phi}^{\text{SrTiO}_3}$.

Gibbs potential coefficients are renormalized by the surface tension [28, 38], misfit strains [33] and biquadratic coupling between the structural and polar order parameters [30, 38-32]. The renormalization details are listed in **Appendix A, Suppl. Mat.[45]** The material parameters are listed in **Table S1, Suppl. Mat.**⁴⁵ To neglect surface gradient effects in the numerical calculations, we assume that extrapolation lengths are much greater than the film thickness h . To account for possible dislocations, effective misfit strain [46] can be introduced as $u_m^*(h) = u_m$ at $h_d < h$ and $u_m^*(h) = u_m h_d/h$ at $h_d \geq h$, where h_d is the critical thickness for dislocation formation.

III. PHASE DIAGRAMS OF $\text{Eu}_x\text{Sr}_{1-x}\text{TiO}_3$ THIN FILMS: NEW PHASES

Numerical calculations of the $\text{Eu}_x\text{Sr}_{1-x}\text{TiO}_3$ thin films polar, structural properties and phase diagrams were performed as a function of temperature T , composition x and misfit strain u_m^* . The

phase diagrams of $\text{Eu}_x\text{Sr}_{1-x}\text{TiO}_3$ bulk and thin films are presented in **Figures 2-4**. It should be noted that the gradient effects, which may appear in the vicinity of surfaces and domain boundaries, are ignored here for the calculation of homogeneous $\text{Eu}_x\text{Sr}_{1-x}\text{TiO}_3$ films. For the same reason, poorly known polarization and tilt gradient coefficients as well as the flexoelectric effect tensor of EuTiO_3 are not included.

Designation $P_i\Phi_j$ in **Figures 2-4** represents the nonzero components of order parameters in a given phase. For instance $P_3\Phi_3$ corresponds to the tetragonal phase with $P_3 \neq 0$ and $\Phi_3 \neq 0$. The abbreviation ‘‘ortho’’ stands for the orthorhombic phase with $P_1 = P_2 \neq 0$ and $\Phi_1 = \Phi_2 \neq 0$. The abbreviation ‘‘mono’’ stands for the low symmetry monoclinic phase with $P_1 \neq P_2 \neq 0$ and $\Phi_1 = \Phi_2 \neq 0$. The abbreviation ‘‘para’’ stands for the paraelectric non-ferrodistortive phase. The boundary between AFD phases Φ_1 and Φ_3 is indicated by a thick dashed line.

The temperature-composition phase diagrams of $\text{Eu}_x\text{Sr}_{1-x}\text{TiO}_3$ bulk, unstrained ($u_m=0$), weakly strained ($|u_m| \leq 0.01\%$) and strongly strained ($|u_m| = 2\%$) thin films are shown in **Figures 2a, 2b** and **2c-d**, respectively. Two features were observed in these phase diagrams, namely a morphotropic-like boundary between AFD in-plane and out-of-plane phases and a thermodynamically stable ferroelectric monoclinic phase.

The boundary between AFD phases Φ_1 and Φ_3 in the weakly strained films only, i.e. at $|u_m| \leq 0.01\%$, is morphotropic-like, and the film becomes spontaneously twinned. Note that the phases Φ_1 and Φ_3 are indistinguishable in the bulk since they are essentially the two variants of the tetragonal phase which are energetically equivalent. However, biaxial stresses exist in the thin epitaxial films clamped to a rigid substrate even at zero misfit strain (see **Appendix A, Suppl. Mat.**⁴⁵). However, the biaxial stress leads to the renormalization of the coefficients $\beta_{\rho_{ij}}^*$ and $\beta_{\Phi_{ij}}^*$. Since $\alpha_{\Phi_i}^* = \alpha_{\Phi_i}$ at $u_m = 0$ according to Eq.(2), the symmetry between the in-plane and out-of-plane directions is broken. Thus, the AFD phases with the order parameter pointed along these two directions become thermodynamically non-equivalent.

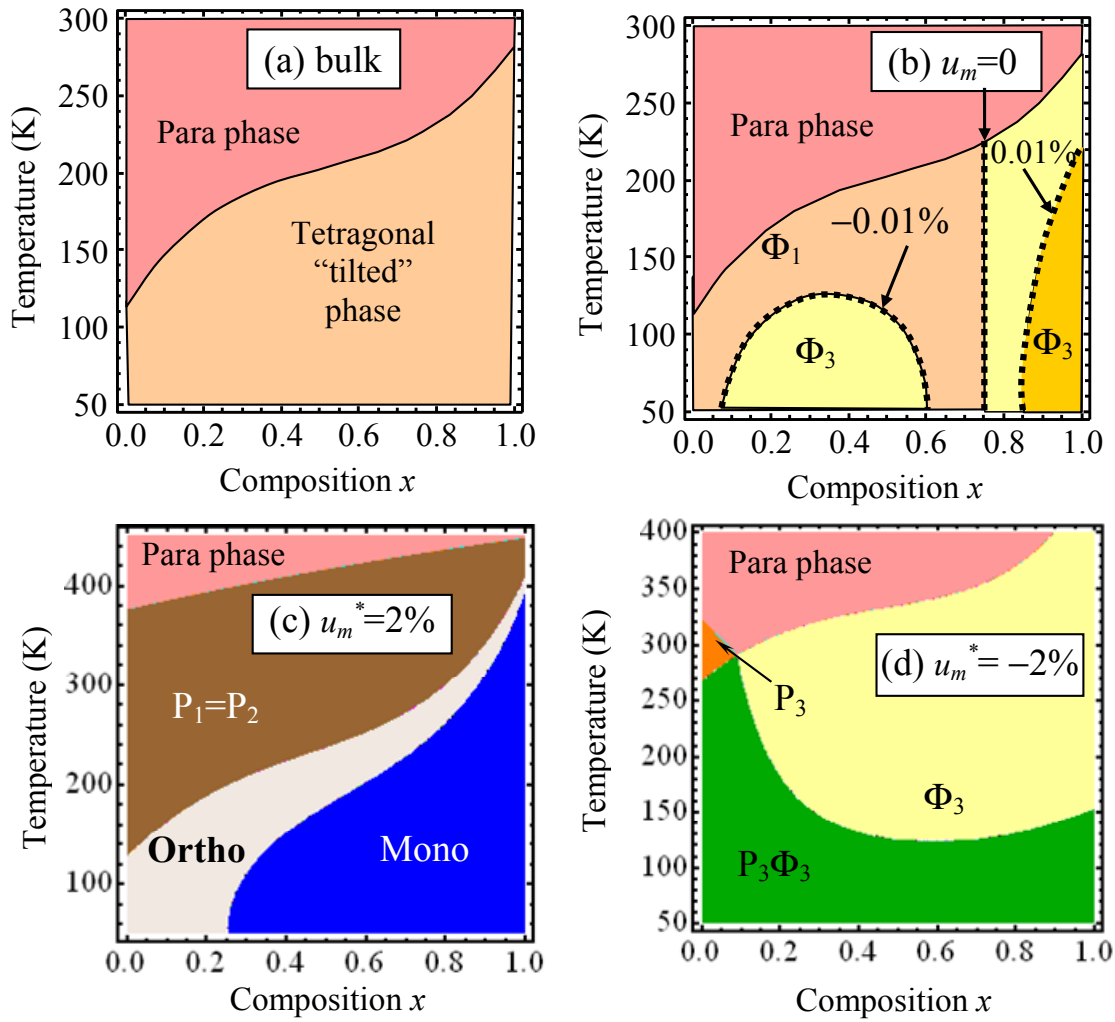


Figure 2. Temperature - composition phase diagrams of $\text{Eu}_x\text{Sr}_{1-x}\text{TiO}_3$ bulk **(a)** and thin films **(b-d)**. Plot **(b)** is calculated for the matched substrate corresponding to zero misfit $u_m=0$ (vertical boundary Φ_1/Φ_3), $u_m^*=-0.01\%$ (left Φ_3 region), $u_m^*=+0.01\%$ (right Φ_3 region). Plots **(c-d)** correspond to misfits $u_m^*=+2\%$ **(c)**, $u_m^*=-2\%$ **(d)**.

$\text{Eu}_x\text{Sr}_{1-x}\text{TiO}_3$ films phase diagrams are mainly in-line with the earlier theoretical calculations for SrTiO_3 [7, 12] and experiment [47], as well as for EuTiO_3 *ab initio* calculations [24] and experiments [25, 26]. It is well-known that tensile strains induce in-plane ferroelectric polarization in both SrTiO_3 [7, 12] and EuTiO_3 [24, 25]. Several theoretical studies [7, 12] predicted that compressive strains can induce out-of-plane tetragonal ferroelectric phase in SrTiO_3 . Jang et al. confirmed the ferroelectricity in SrTiO_3 films on a (110) NdGaO_3 substrate with an average biaxial compressive strain of -1.18% under a fully commensurate condition. The absence of ferroelectricity in SrTiO_3 films grown on compressive $(\text{La,Sr})(\text{Al,Ta})\text{O}_3$ (LSAT) substrates, the lattice constant of which is close to that of NdGaO_3 , may be related to the increase of AFD transition temperature [48]. Different polar properties of $\text{SrTiO}_3/\text{LSAT}$ and $\text{SrTiO}_3/\text{NdGaO}_3$ may

originate from the strong structural anisotropy of orthorhombic NdGaO_3 in comparison with cubic LSAT substrates.

Despite the agreement with the phenomenological studies [7, 12], we have found one important difference in SrTiO_3 thin films. In particular, Pertsev et al. [7] predicted the existence of both pure AFD phases and AFD-FE phases in homogeneous epitaxial SrTiO_3 films (see fig. 1 in the paper). However, they did not report any monoclinic phases. From our calculations, an ultra-thin monoclinic region of the low symmetry monoclinic phase appears at tensile strains more than 1% for pure SrTiO_3 (see **Figure 3a,b**).

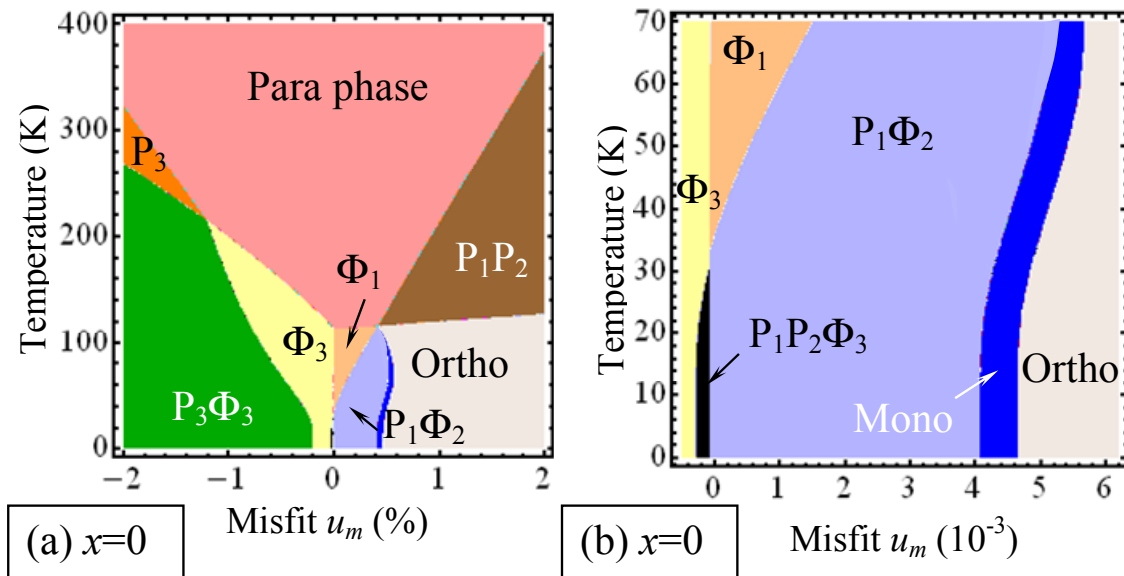


Figure 3. Temperature - misfit strain phase diagrams of SrTiO_3 thin films for a wide range of misfit strain (a) and for its small values (b).

The appearance of the monoclinic phase in SrTiO_3 and $\text{Eu}_x\text{Sr}_{1-x}\text{TiO}_3$ may, at first glance, seem contradictory to the Vanderbilt and Cohen result [49]. According to them, a monoclinic phase can be thermodynamically stable only when the corresponding Landau expansion includes terms of 8th order or higher in polarization while our Gibbs potential only includes 4th order terms. However, there are key differences between the thermodynamic conditions considered in the work by Vanderbilt and Cohen and in this work. First of all, Vanderbilt and Cohen considered a homogenous single domain state under a stress-free condition while we consider a thin film under a biaxial strain. Secondly, Vanderbilt and Cohen arrived at their conclusion by analyzing the dependence of the Landau free energy on the orientation of a 3-component vector order parameter with a fixed magnitude, while we minimize the free energy of a strained film with respect to both the directions and magnitudes of two order parameters, namely, polarization and rotation, i.e., a

total of six components. Therefore, our results reported here are not contradictory to those of Vanderbilt and Cohen.

Minimization of the free energy (A.4) with respect to P_i and Φ_i leads to a system of six coupled cubic equations (A.8) in the case of homogeneous film [⁴⁵]. We derived the analytical expressions for the order parameters in the monoclinic phase with polarization components $P_1 \neq P_2 \neq 0$ and tilts $\Phi_1 \neq \Phi_2 \neq 0$ [**Appendix B, Suppl. Mat.** ⁴⁵]. The degree of “monoclinicity” was calculated analytically as

$$P_1^2 - P_2^2 = a_m \sqrt{\frac{P_m^4 - \phi^2 \Phi_m^4}{a_m^2 - \phi^2}}, \quad \Phi_1^2 - \Phi_2^2 = \sqrt{\frac{P_m^4 - \phi^2 \Phi_m^4}{a_m^2 - \phi^2}}, \quad (5)$$

where $P_m \equiv \sqrt{P_1^2 + P_2^2}$ and $\Phi_m \equiv \sqrt{\Phi_1^2 + \Phi_2^2}$. Evident expressions for a_m , ϕ^2 , Φ_m and P_m are given in **Appendix B.** ⁴⁵

The stability of monoclinic phase (i.e. its minimal energy) was examined by the minimization of the $\text{Eu}_x\text{Sr}_{1-x}\text{TiO}_3$ free energy (A.4) with respect to P_1, P_2 and Φ_1, Φ_2 without any additional assumptions. The reason why monoclinic phase is ignored by previous studies might be the assumption that $|P_1| = |P_2|$ or/and $|\Phi_1| = |\Phi_2|$. Initially we tried to use the assumption, but found the region on the phase diagram with non-physical negative dielectric susceptibility, which indicates the instability. Furthermore, our numerical calculations indeed showed that the monoclinic phase with $|P_1| \neq |P_2| \neq 0$ and $|\Phi_1| \neq |\Phi_2| \neq 0$ is thermodynamically stable in the region.

One can see from **Figures 4** that the monoclinic phase region is strongly dependent on Eu content x and temperature. **Figures 4a-d** show phase diagrams of $\text{Eu}_x\text{Sr}_{1-x}\text{TiO}_3$ thin films in the coordinates of misfit strain–composition (plots **a,b**) and temperature - misfit strain (plots **c,d**). The boundary Φ_1/Φ_3 occurs at very small misfit strains $|u_m| \leq 0.01\%$ and is almost independent of composition until the transition from the AFD to para-phase takes place. The para-phase region increases with temperature (compare **Figs. 4a** and **4b**). Different orthorhombic phases ($P_1 = P_2 \neq 0$ and $\Phi_1 = \Phi_2 \neq 0$, and $P_1 = P_2 \neq 0$) dominate at small x . As x increases, the monoclinic phase replaces the orthorhombic phase region. The monoclinic phase exists in tensile strained EuTiO_3 films ($u_m \approx 2\%$) up to temperatures 400 K and higher.

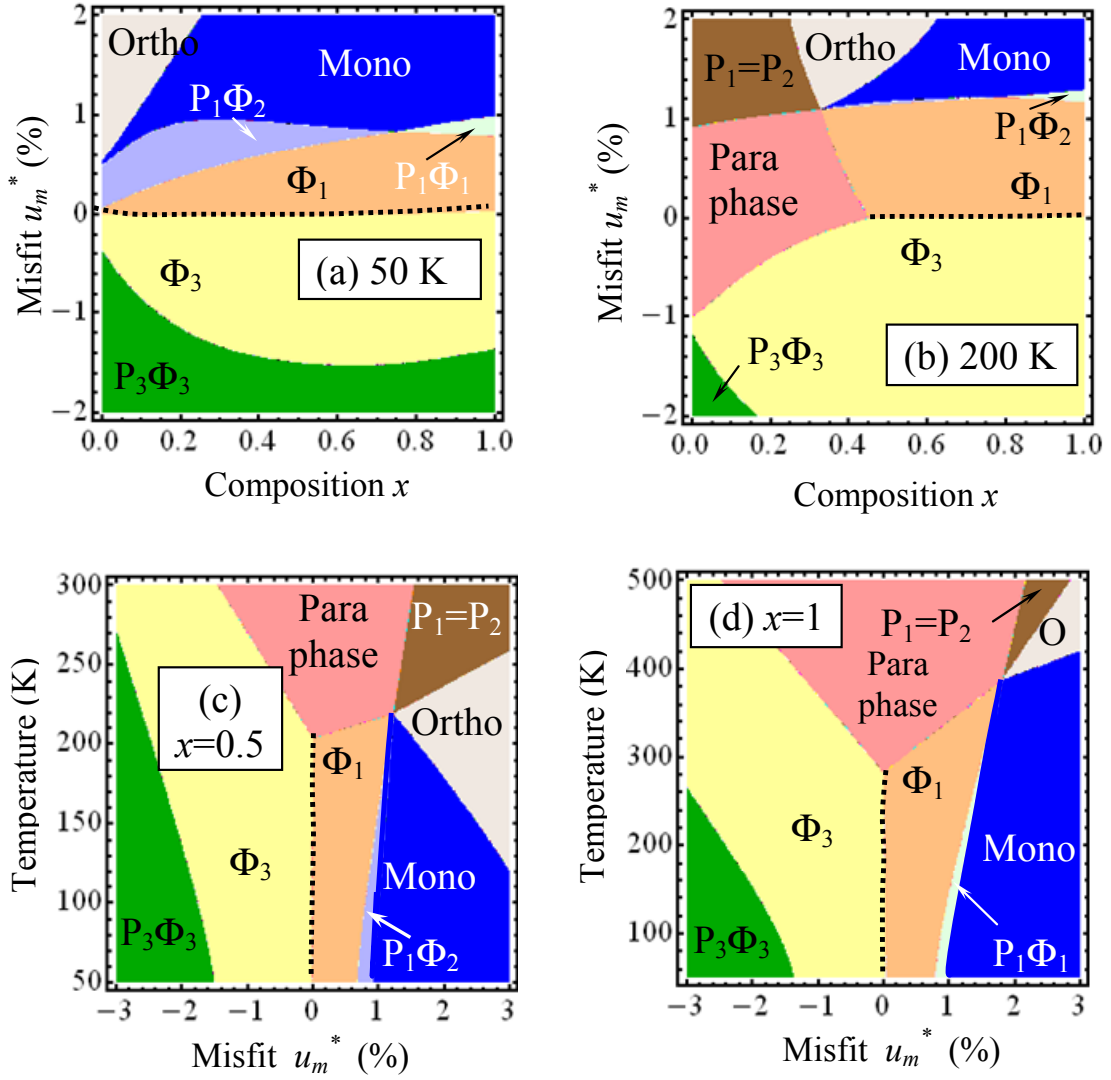


Figure 4. The misfit strain–composition phase diagrams of $\text{Eu}_x\text{Sr}_{1-x}\text{TiO}_3$ thin films at temperature 50 K **(a)** and 200 K **(b)**. Temperature - misfit strain phase diagrams of the films of composition $x=0.5$ **(c)** and $x=1$ **(d)**.

Note, that at a particular composition, the free energy is a function of temperature, biaxial strain, and 6 order parameter components, and hence the multiphase (4-5) junctions in the phase diagrams in **Figure 3a** and **Figures 4** are thermodynamically possible. The Gibbs phase rule is violated as not applicable for the case [50]. Existing publications have also shown such multiphase junctions, e.g., 5 phases can meet in one point in the SrTiO_3 phase diagram [7] and [51].

One can see from **Figures 5a,b** that the linear dielectric permittivity demonstrates typical peculiarities (jump or divergences) near the phase transitions. Nonzero component of permittivity tensor ϵ_{12} and the condition $\epsilon_{11} \neq \epsilon_{22} \neq \epsilon_{33}$ are the unique features of the monoclinic phase realization in the tensile-strained $\text{Eu}_x\text{Sr}_{1-x}\text{TiO}_3$ films. The dielectric anisotropy factors $\epsilon_{11}/\epsilon_{22}$ and

$\epsilon_{22}/\epsilon_{33}$ range from several to several hundreds of times for the $\text{Eu}_{0.5}\text{Sr}_{0.5}\text{TiO}_3$ films with effective misfit strain $u_m^* = +1\%$, meaning the monoclinicity can strongly affect the anisotropy of dielectric permittivity. Temperature dependence of piezoelectric constants in the monoclinic phase ($0 < T < 380$ K) of tensile-strained EuTiO_3 film is shown in **Figure 5c**. The values characterize the piezoelectric response of a single-domain film. Some components of piezoelectric response are drastically enhanced in the vicinity of the twin walls (**Figure 5d**), indicating the possible appearance of new highly tunable states in incipient ferroelectrics.

Note, that temperature dependence of dielectric permittivity of $\text{Eu}_{0.5}\text{Sr}_{0.5}\text{TiO}_3$ shown in **Figures 5a,b,c** are calculated for the homogeneous films without gradient effects and thus does not require information about polarization, tilt gradient coefficients, and the flexoelectric effect tensor of EuTiO_3 , which are currently unknown. The quantitative validity of the profiles of piezoelectric response components calculated across the twin walls and shown in **Figure 5d** is under question because we used the gradient and flexoelectric coefficients of SrTiO_3 to generate the curves. However we believe that **Figure 5d** is at least qualitatively correct because the values of flexoelectric coefficients measured experimentally for SrTiO_3 by Zubko et al [39] are in a reasonable agreement with microscopic theoretical estimations made by Kogan [52], as well as with recent DFT calculations for other ferroelectric perovskites [53, 54]. In other words one can expect that the flexoelectric tensor should not differ much for perovskites SrTiO_3 and EuTiO_3 .

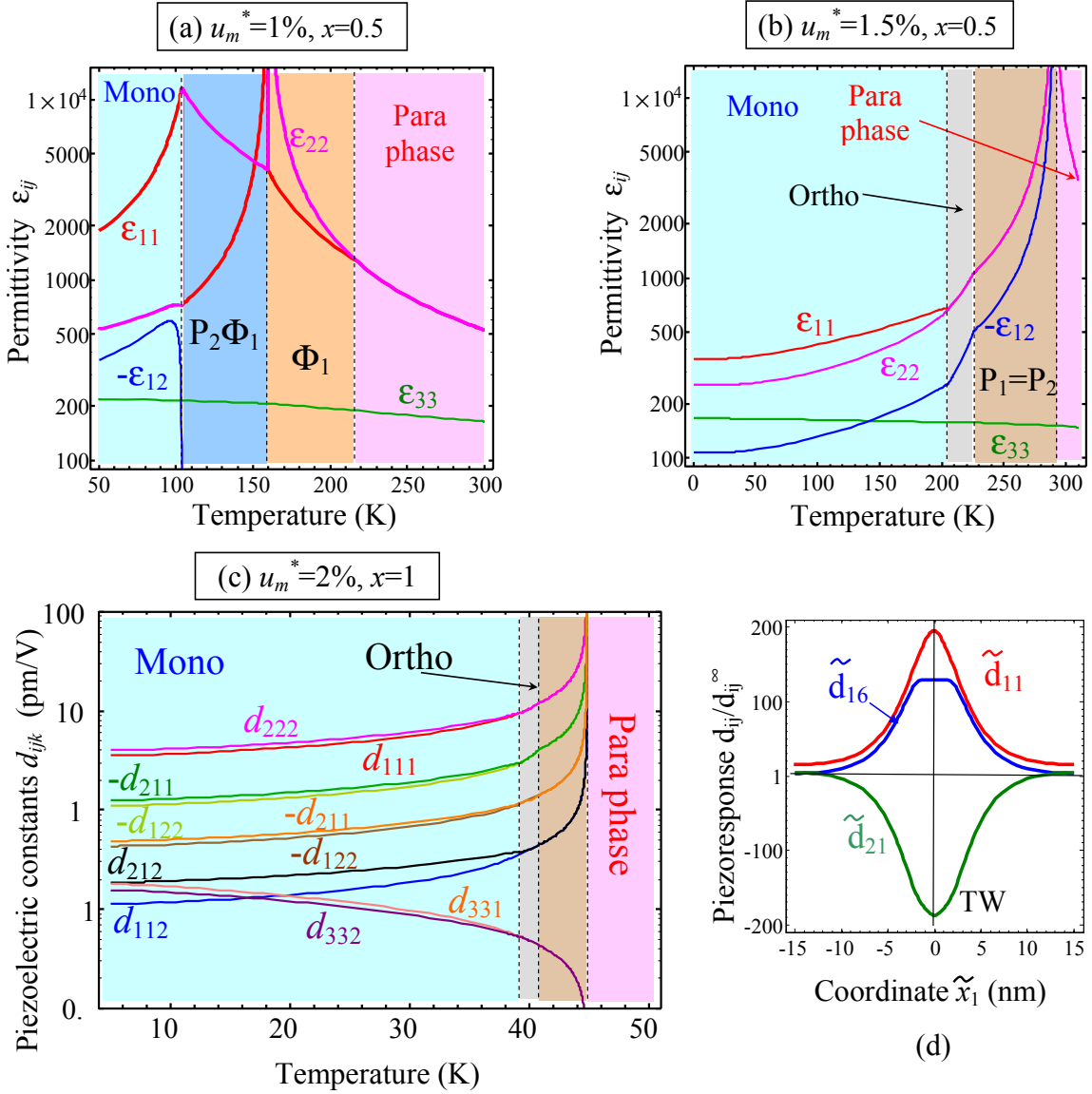


Figure 5. Temperature dependence of dielectric permittivity of $\text{Eu}_{0.5}\text{Sr}_{0.5}\text{TiO}_3$ films calculated for tensile misfit strains $u_m^* = +1\%$ (a), $u_m^* = +1.5\%$ (b). Temperature dependence of piezoelectric constants of tensiled EuTiO_3 film, $u_m^* = +2\%$ (c). Different phases are separated by the vertical lines. Phase designations are the same as in **Figure 4**. Schematic profiles of several piezoelectric response components across the twin walls (d).

Our calculations show that the favourable condition of the monoclinic phase appearance in $\text{Eu}_x\text{Sr}_{1-x}\text{TiO}_3$ is the *negative sign* of biquadratic coupling tensor coefficients ξ_{ik} (see **Table 1**). Also LGD-expansion coefficients $\alpha_{p_i}^*$ and $\alpha_{\phi_i}^*$ should be negative. But these conditions could be readily reached in the strained films since the coefficients are essentially renormalized by misfit strains. The conditions $\xi_{ij}^* < 0$ are valid if $\xi_{ij} < 0$ because the renormalization of ξ_{ik} by misfit

effect is usually small. The opposite signs of the coupling tensor ξ_{ik} in SrTiO₃ and EuTiO₃ can explain the increase of the monoclinic phase region with the increase of Eu content, x . Thus we can conclude that simultaneous presence of both octahedra tilts and polarization in epitaxial Eu _{x} Sr_{1- x} TiO₃ films stabilize in-plane monoclinic phase at moderate and high tensile strains $u_m > 1\%$.

Table 1. Biquadratic coupling type with respect to the monoclinic phase origin

AFD material	Biquadratic coupling type	Refs.
SrTiO ₃	unfavourable	e.g. [7]
EuTiO ₃	favourable	Our fit
CaTiO ₃	unfavourable	Yijia Gu et al. [5]
PbZr _{x} Ti _{1-x} O ₃	favourable	Haun et al. [40]

It should be noted that the monoclinic phase can also appear as the intermediate phase between the phases with higher order symmetry [55]. For example, the monoclinic phase was found in Pb(Zr,Ti)O₃ by Noheda et al. [56] at the morphotropic boundary between tetragonal and rhombohedral phases. It was demonstrated [57] that the monoclinic phase in Pb(Zr,Ti)O₃ is accompanied by the octahedral tilts, at least at lower temperatures. Local inhomogeneity can stabilize monoclinic phase as well. The monoclinic phase was predicted in the superlattices BaTiO₃/SrTiO₃ [58] as a consequence of complex electrostatic and elastic interactions within an inhomogeneous domain structure in the multilayered ferroelectric film.

IV. FLEXO-ROTO EFFECTS AT ELASTIC TWINS IN Eu _{x} Sr_{1- x} TiO₃

The monoclinic phase is characterized by the high number of energetically equivalent tilt and polarization domain variants, leading to no less than 16 types of twins, consisting of 8 ferroelectric twin pairs with different orientations of tilt vector. High number of possible domain pairs (mostly twins) results in easy twinning of a strained film, and consequently enhance the piezoelectric response and electromechanical tunability.

The film becomes spontaneously twinned in the vicinity of morphotropic boundaries Φ_1/Φ_3 as well as in the monoclinic phase with $P_1 \neq P_2 \neq 0$ and $\Phi_1 \neq \Phi_2 \neq 0$. Due to the presence of rotostriction and flexoelectric coupling, spontaneous polarization, piezo- and pyroelectricity may arise from elastic twin boundaries (TB) [30]. Recent experimental measurements [37] seem to confirm these theoretical predictions. For example, Scott et al [37] studied the damping and elastic softening of twin walls in bulk SrTiO₃ and showed that ferroelastic domain walls become ferroelectric at low temperatures.

The joint action of rotostriction and flexoelectric coupling [30] produces the inhomogeneous strain $u_{ij}(\mathbf{r}) \propto R_{mnpq} \partial(\Phi_p \Phi_q) / \partial x_l$ across the structural TB that induces the variation of polarization ($\delta P_i(\mathbf{r})$), piezoelectric ($\delta d_{ijk}(\mathbf{r})$) and pyroelectric ($\delta \Pi_i(\mathbf{r})$) responses as:

$$\delta P_i(\mathbf{r}) \propto -\alpha_{iv}^{-1} f_{mnl} R_{mnpq} \frac{\partial(\Phi_p \Phi_q)}{\partial x_l}, \quad (6a)$$

$$\delta d_{ijk}(\mathbf{r}) \approx 2\epsilon_0 \epsilon_{im} Q_{mkjl} \delta P_l(\mathbf{r}), \quad \delta \Pi_i(\mathbf{r}) = -\gamma_{ij} \frac{\partial}{\partial T} \delta P_j(\mathbf{r}). \quad (6b)$$

where f_{mnl} denotes direct flexoelectric tensor, $f_{ijkl} = c_{ijmn} F_{mnkl}$; γ_{ij} is the pyroelectric coefficients tensor; $\epsilon_0 = 8.85 \times 10^{-12}$ F/m is the universal dielectric constant, ϵ_{ij} is the relative dielectric permittivity. Note, that Eq.(6a) is valid only for zero electric field, including both external and depolarization fields. Estimations based in Eqs.(6) give 0.5–5 C/m² for $\delta P_i(\mathbf{r})$, 10 pm/V for $\delta d_{ijk}(\mathbf{r})$ and (5–50)10⁻⁶ C/m²K for $\delta \Pi_i(\mathbf{r})$ depending on temperature and content x. The numerical values are in agreement with previous studies of roto-flexo effect [30, 31, 32]. Note, that there are other possible reasons for polar surface states in nonpolar materials such as SrTiO₃, such as surface piezoelectricity [59, 60, 61, 62]. For example, Dai et al [62] obtained surface polarization $\sim(0.07 - 0.02) \mu\text{C}/\text{cm}^2$ for SrTiO₃ in a wide temperature range. However, the roto-flexo effect can lead to higher polarization values $\sim(0.5-5) \mu\text{C}/\text{cm}^2$ in the AFD phase.

The spontaneous polarization induced by the tilt gradient in the vicinity of SrTiO₃ TB was obtained by the phase-field modelling. Profiles of the tilts $\tilde{\Phi}_1$ and $\tilde{\Phi}_2$, polarization \tilde{P}_1 and \tilde{P}_2 components calculated across the easy and hard TB are presented in **Figure 6**. The calculations were performed in the rotated frame $\{\tilde{x}_1, \tilde{x}_2\}$ shown in the **Figure 6b**. For **hard TB**, \tilde{P}_1 is odd and \tilde{P}_2 is even (see **Figures 6c-d**). The even Bloch-type component \tilde{P}_2 flips when $\tilde{\Phi}_1$ flips, as one can conclude comparing the plots (c) and (d). The magnitude of \tilde{P}_1 and \tilde{P}_2 are quite different, and this is similar to the hard antiphase boundaries [30]. For **easy TB** \tilde{P}_1 is odd and \tilde{P}_2 is even (see **Figures 6e-f**). The even \tilde{P}_2 flips when $\tilde{\Phi}_2$ flips, as one can see comparing the plots (e) and (f). The magnitudes of \tilde{P}_1 and \tilde{P}_2 are similar. These results are in a semi-quantitative agreement with previous analytical results [30]. However, one interesting parity-related effect that was not reported previously is evident. It is the flip of the even Bloch-type polarization distribution \tilde{P}_2 with the sign change of the Ising-type tilt component $\tilde{\Phi}_1$. At the same time the odd component of polarization profile is independent of the tilt sign. The result can be explained by analysing the symmetry of the inhomogeneous strains $\tilde{u}_{ij}(\mathbf{r}) \propto \tilde{R}_{mnpq} \partial(\tilde{\Phi}_p \tilde{\Phi}_q) / \partial \tilde{x}_l$, which are responsible for the

appearance of components \tilde{P}_1 and \tilde{P}_2 in the vicinity of TB. The origin for the polarization components are $\tilde{P}_1 \propto \partial(\tilde{\Phi}_1^2)/\partial\tilde{x}_1$ and $\tilde{P}_2 \propto \partial(\tilde{\Phi}_1\tilde{\Phi}_2)/\partial\tilde{x}_1$ according to the Euler-Lagrange equations [30]. Therefore, \tilde{P}_1 is the even function of $\tilde{\Phi}_1$, and \tilde{P}_2 is the odd function of $\tilde{\Phi}_1$.

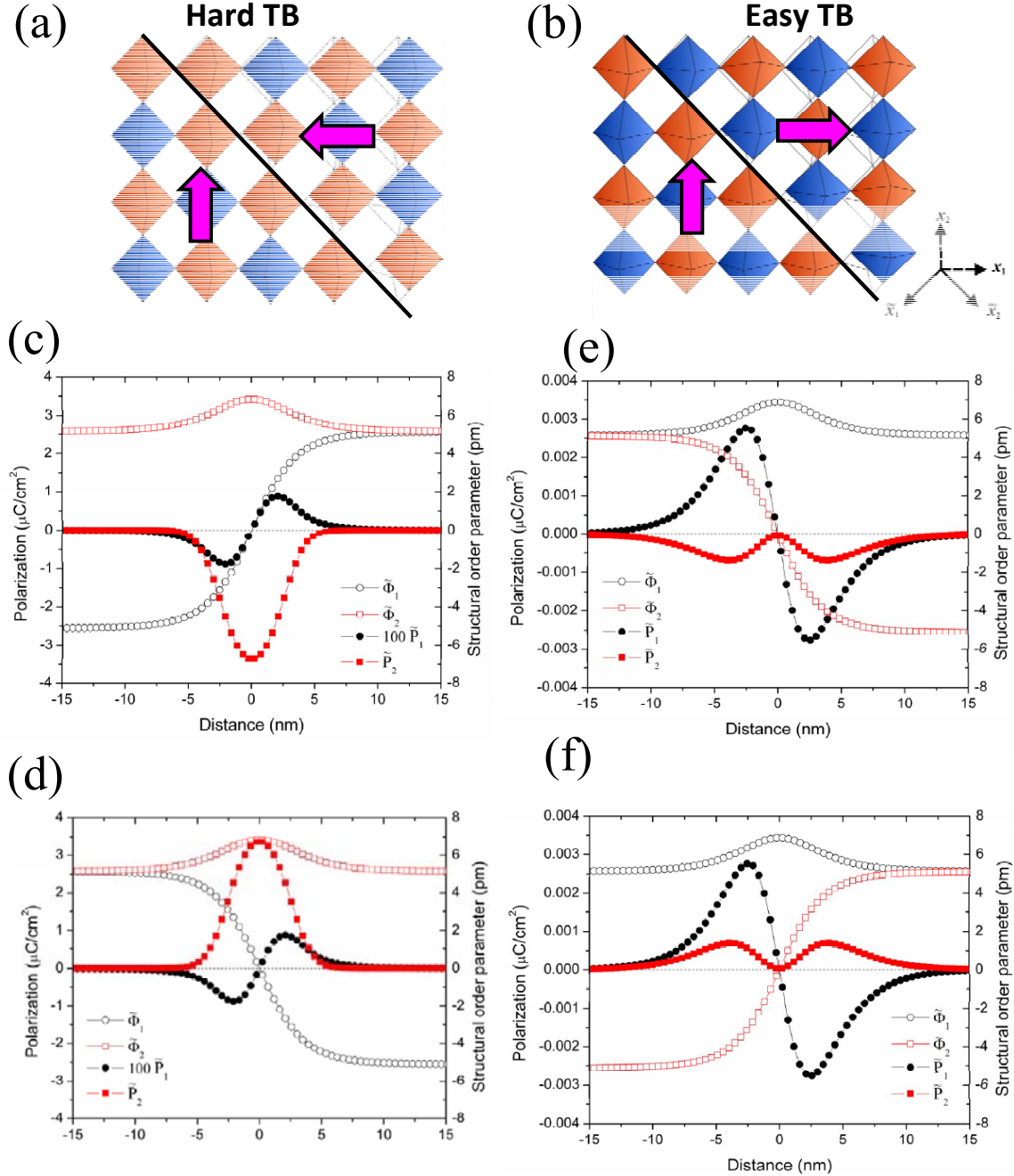


Figure 6. (a) Configuration of oxygen octahedrons tilt across the “head-to-head” hard TB. (b) Configuration of oxygen octahedrons tilt across the “head-to-tail” easy TB. (c-f) The spontaneous polarization induced by the tilt gradient in the vicinity of the TB. Results are calculated by the phase-field modelling for SrTiO₃ parameters.

Note that there were misprints in the gradient coefficients in Ref.[5]. Corrected set of SrTiO₃ coefficients is given in the **Table S1, Suppl. Mat.** [63]. Using the set of parameters from **Table S1**⁴⁵ we found that two kinds of twin boundaries have similar wall width (compare left and right column in the **Figure 6**).

V. SUMMARY

Using Landau-Ginzburg-Devonshire 2-4-power expansion and phase-field modelling, we studied the interplay between the long-range structural order parameter and polarization in epitaxial Eu_xSr_{1-x}TiO₃ thin films.

A new low symmetry ferroelectric monoclinic phase is shown to become stable in Eu_xSr_{1-x}TiO₃ thin films at moderate tensile strains. We derived analytical expressions for the spontaneous tilt and ferroelectric polarization vectors for the monoclinic phase and demonstrated that the presence of antiferrodistortive octahedra tilts stabilizes the monoclinic phase with in-plane ferroelectric polarization. The monoclinic phase region is strongly dependent on the Eu content. It is also shown that the monoclinic phase is thermodynamically stable in a wide temperature range. The monoclinic phase is characterized by a large number of energetically equivalent orientations of the polar and structural order parameters. Since the local elastic field gradients of adjacent domain walls will interact, the appearance of highly tunable piezoelectricity in the incipient ferroelectric films is possible while it is not expected in the corresponding bulk Eu_xSr_{1-x}TiO₃. Using phase-field modelling we demonstrate that the flexoelectric coupling and rotostriction give rise to the spontaneous polarization at the elastic twin boundaries due to the intrinsic strain gradient. The interfacial polarization displays an interesting parity-related effect, namely, changing the sign of the Ising-type tilt component leads to the flip of the Bloch-type polarization distribution.

Acknowledgements: A.N.M. M.D.G., V.V.K and E.A.E. acknowledge State Fund of Fundamental State Fund of Fundamental Research of Ukraine, SFFR-NSF project UU48/002. Y.G, V.G. and L.Q.C. acknowledge the financial supports by the US National Science Foundation under NSF-DMR- 0908718, NSF-DMR-0820404, and NSF-DMR-1210588.

References

- 1 Darrell G. Schlom, Long-Qing Chen, Chang-Beom Eom, Karin M. Rabe, Stephen K. Streiffer, and Jean-Marc Triscone. *Annu. Rev. Mater. Res.* **37**, 589–626 (2007).
- 2 D.D. Fong, G.B. Stephenson, S.K. Streiffer, J.A. Eastman, O. Auciello, P.H. Fuoss, and C. Thompson, *Science* **304**, 1650 (2004).
- 3 M. J. Highland, T. T. Fister, D. D. Fong, P. H. Fuoss, Carol Thompson, J. A. Eastman, S. K. Streiffer, and G. B. Stephenson. *Phys. Rev. Lett.* **107**, 187602 (2011)
- 4 Ying-Hao Chu, Lane W. Martin, Mikel B. Holcomb, Martin Gajek, Shu-Jen Han, Qing He, Nina Balke, Chan-Ho Yang, Donkoun Lee, Wei Hu, Qian Zhan, Pei-Ling Yang, Arantxa Fraile-Rodríguez, Andreas Scholl, Shan X. Wang & R. Ramesh. *Nature Materials* **7**, 478 - 482 (2008)
- 5 Yijia Gu, Karin Rabe, Eric Bousquet, Venkatraman Gopalan, and Long-Qing Chen. *Phys. Rev. B* **85**, 064117 (2012).
- 6 Yurong Yang, Wei Ren, Massimiliano Stengel, X. H. Yan, and L. Bellaiche. *Phys. Rev. Lett.* **109**, 057602 (2012).
- 7 N. A. Pertsev, A. K. Tagantsev, and N. Setter, *Phys. Rev. B* **61**, R825 (2000).
- 8 W. Cao and R. Barsch, *Phys. Rev. B*, **41**, 4334 (1990)
- 9 P. A. Fleury, J. F. Scott, and J. M. Worlock. Soft Phonon Modes and the 110°K Phase Transition in SrTiO₃. *Phys. Rev. Lett.* **21**, 16–19 (1968)
- 10 P.A. Fleury and J. M. Worlock. *Phys. Rev.* **174**, 613 (1968).
- 11 A.K. Tagantsev, E. Courtens and L. Arzel, *Phys. Rev. B*, **64**, 224107 (2001).
- 12 J. H. Haeni, P. Irvin, W. Chang, R. Uecker, P. Reiche, Y. L. Li, S. Choudhury, W. Tian, M. E. Hawley, B. Craigo, A. K. Tagantsev, X. Q. Pan, S. K. Streiffer, L. Q. Chen, S. W. Kirchoefer, J. Levy, D. G. Schlom. *Nature* **430**, 758 (2004).
- 13 Y. L. Li, S. Choudhury, J. H. Haeni, M. D. Biegalski, A. Vasudevarao, A. Sharan, H. Z. Ma, J. Levy, Venkatraman Gopalan, S. Trolier-McKinstry, D. G. Schlom, Q. X. Jia, and L. Q. Chen. *Phys. Rev. B* **73**, 184112 (2006).
- 14 A. Ohtomo and H.Y. Hwang. *Nature*, **427**, 423-426 (2004).
- 15 R. Oja, M. Tyunina, L. Yao, T. Pinomaa, T. Kocourek, A. Dejneka, O. Stupakov, M. Jelinek, V. Trepakov, S. van Dijken, and R. M. Nieminen. *Phys. Rev. Lett.* **109**, 127207 (2012).
- 16 Y. Y. Guo, H. M. Liu, D. P. Yu, and J.-M. Liu. *Phys. Rev. B* **85**, 104108 (2012)
17. T. Katsufuji and H. Takagi, *Phys. Rev. B* **64**, 054415 (2001).
18. V. V. Shvartsman, P. Borisov, W. Kleemann, S. Kamba, T. Katsufuji. *Phys. Rev. B* **81**, 064426 (2010).

-
- 19 A. Bussmann-Holder, J. Kohler, R. K. Kremer, and J. M. Law. *Phys. Rev. B* **83**, 212102 (2011).
- 20 Mattia Allieta, Marco Scavini, Leszek Spalek, Valerio Scagnoli, Helen C. Walker, Christos Panagopoulos, Siddharth Saxena, Takuro Katsufuji and Claudio Mazzoli. *Phys. Rev. B* **85**, 184107 (2012).
- 21 K. Z. Rushchanskii, N. A. Spaldin, and M. Lezaic. *Phys. Rev. B* **85**, 104109 (2012).
22. V. Goian, S. Kamba, O. Pacherova, J. Drahokoupil, L. Palatinus, M. Dusek, J. Rohlíček, M. Savinov, F. Laufek, W. Schranz, A. Fuith, M. Kachlík, K. Maca, A. Shkabko, L. Sagarna, A. Weidenkaff, and A. A. Belik. *Phys. Rev. B* **86**, 054112 (2012).
- 23 A. P. Petrović, Y. Kato, S. S. Sunku, T. Ito, P. Sengupta, L. Spalek, M. Shimuta T. Katsufuji, C. D. Batista, S. S. Saxena, and C. Panagopoulos. *Phys. Rev. B* **87**, 064103 (2013).
24. C.J. Fennie, & K.M. Rabe, *Phys. Rev. Lett.* **97**, 267602 (2006).
25. J.H. Lee, Lei Fang, Eftihia Vlahos, Xianglin Ke, Young Woo Jung, L.F. Kourkoutis, Jong-Woo Kim, P.J. Ryan, Tassilo Heeg, M. Roeckerath, V. Goian, M. Bernhagen, R. Uecker, P.C. Hammel, K.M. Rabe, S. Kamba, J. Schubert, J.W. Freeland, D.A. Muller, C.J. Fennie, P. Schiffer, V. Gopalan, E. Johnston-Halperin, D. Schlom. *Nature*, **466**, 954, (2010) doi: 10.1038/nature09331
- 26 P.J. Ryan, J.-W. Kim, T. Birol, P. Thompson, J.-H. Lee, X. Ke, P.S. Normile, E. Karapetrova, P. Schiffer, S.D. Brown, C.J. Fennie, D.G. Schlom, *Nat. Commun.* **4**, 1334 (2013)
- 27 Zurab Guguchia, Alexander Shengelaya, Hugo Keller, Jurgen Kohler, and Annette Bussmann-Holder. *Phys. Rev. B* **85**, 134113 (2012).
- 28 Eugene A. Eliseev, Maya D. Glinchuk, Victoria V. Khist, Chan-Woo Lee, Chaitanya S. Deo, Rakesh K. Behera, and Anna N. Morozovska. *J. Appl. Phys.* **113**, 024107 (2013).
- 29 V. Gopalan and D.B. Litvin, *Nature Materials* **10**, 376–381 (2011).
- 30 A.N. Morozovska, E.A. Eliseev, M.D. Glinchuk, Long-Qing Chen, Venkatraman Gopalan. *Phys.Rev.B.* **85**, 094107 (2012).
- 31 A.N. Morozovska, E.A. Eliseev, S.V. Kalinin, Long-Qing Chen and Venkatraman Gopalan. *Appl. Phys. Lett.* **100**, 142902 (2012)
- 32 A.N. Morozovska, E.A. Eliseev, S.L. Bravina, A.Y. Borisevich, and S.V. Kalinin. *J. Appl. Phys.* **112**, 064111 (2012)
- 33 N.A. Pertsev, A.G. Zembilgotov, A. K. Tagantsev. *Phys. Rev. Lett.* **80**, 1988 (1998).
- 34 Oswaldo Diéguez, Silvia Tinte, A. Antons, Claudia Bungaro, J. B. Neaton, Karin M. Rabe, and David Vanderbilt. *Phys. Rev. B* **69**, 212101 (2004).
- 35 Y.L. Li, L. Q. Chen. *Appl. Phys. Lett.* **88**, 072905 (2006).

-
- 36 Eugene A. Eliseev, Anna N. Morozovska, Yijia Gu, Albina Y. Borisevich, Long-Qing Chen and Venkatraman Gopalan, and Sergei V. Kalinin. *Phys.Rev. B* **86**, 085416 (2012)
- 37 J. F. Scott, E. K. H. Salje, M. A. Carpenter. *Phys. Rev. Lett.* **109**, 187601 (2012).
- 38 A.N. Morozovska, M. D. Glinchuk, Rakesh K. Behera, B. Zaulychny, Chaitanya S. Deo, E.A. Eliseev. *Phys. Rev.* **B 84**, 205403 (2011).
- 39 P. Zubko, G. Catalan, A. Buckley, P.R. L. Welche, J. F. Scott. *Phys. Rev. Lett.* **99**, 167601 (2007).
- 40 M. J. Haun, E. Furman, T. R. Halemane and L. E. Cross, *Ferroelectrics*, **99**, 55 (1989), *ibidem* p.13.
41. B. Houchmanzadeh, J. Lajzerowicz and E Salje, *J. Phys.: Condens. Matter* **3**, 5163 (1991).
- 42 M. Daraktchiev, G. Catalan, J. F. Scott, *Ferroelectrics*, **375**, 122 (2008).
- 43 J. H. Barrett, *Phys. Rev.* **86**, 118 (1952)
- 44 A. Bussmann-Holder, private communication (2012).
- 45 See Supplemental Material at [URL will be inserted by publisher] for calculations details
- 46 J.S. Speck, W. Pompe. *J.Appl.Phys.* **76**(1), 466 (1994).
- 47 H. W. Jang, Amit Kumar, Sava Denev, Michael D. Biegalski, Petro Maksymovych, C. W. Bark, Craig T. Nelson, C. M. Folkman, S. H. Baek, N. Balke, C. M. Brooks, D. A. Tenne, D. G. Schlom, L. Q. Chen, X. Q. Pan, S.V. Kalinin, V. Gopalan, and C. B. Eom. *Physical Review Letters* **104**, 197601 (2010).
- 48 T. Yamada, T. Kiguchi, A. K. Tagantsev, H. Morioka, T. Iijima, H. Ohsumi, S. Kimura, M. Osada, N. Setter, and H. Funakubo. *Integrated Ferroelectrics* **115**, no. 1: 57-62 (2010).
- 49 David Vanderbilt and Morrel H. Cohen. *Phys. Rev. B* **63** 094108 (2001).
- 50 William C. Johnson, On the inapplicability of Gibbs phase rule to coherent solids. *Metallurgical Transactions A* **18**, 1093-1097 (1987)
- 51 N. A. Pertsev, A. K. Tagantsev, and N. Setter, *Phys. Rev. B* **65**, 219901(E) (2002).
- 52 Sh. M. Kogan, *Sov. Phys.—Solid State* **5**, 2069 (1964)
- 53 Jiawang Hong and David Vanderbilt. *Phys. Rev.* **B 84**, 180101(R) (2011)
- 54 I. Ponomareva, A. K. Tagantsev, L. Bellaiche. *Phys.Rev B* **85**, 104101 (2012)
- 55 Makoto Iwata and Yoshihiro Ishibashi. *Japanese Journal of Applied Physics* **44**, No. 5A, pp. 3095–3098 (2005).
- 56 B. Noheda, D. E. Cox, G. Shirane, J. A. Gonzalo, L. E. Cross and S-E. Park. *Appl. Phys. Lett.* **74**, 14, 2059 (1999).
- 57 F. Cordero, F. Trequattrini, F. Craciun and C. Galassi, *J. Phys.: Condens. Matter* **23**, 415901 (2011).

-
- 58 Pingping Wu, Xingqiao Ma, Yulan Li, Venkatraman Gopalan, and Long-Qing Chen. Appl. Phys. Lett. 100, 092905 (2012).
- 59 N. D. Sharma, R. Maranganti, and P. Sharma, Journal of the Mechanics and Physics of Solids **55**, 2328 (2007).
- 60 A. Kholkin, I. Bdikin, T.Ostapchuk, and J.Petzelt, Appl. Phys. Lett. **93**, 222905 (2008).
- 61 N. D. Sharma, C. M. Landis, and P. Sharma, Journal of Applied Physics **108**, 024304 (2010).
- 62 S. Dai, M. Gharbi, P. Sharma, H. S. Park. J. Appl.Phys. **110**, 104305 (2011)
- 63 Note, that there were a misprint in Ref.[28] coefficients